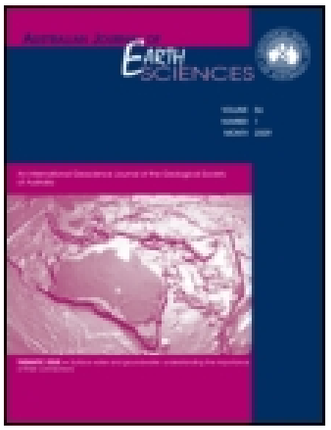

Australian Journal of Earth Sciences: An International Geoscience Journal of the Geological Society of Australia
Publication details, including instructions for authors and subscription information:
http://www.tandfonline.com/loi/taje20

Multiple methods for regional- to mine-scale targeting, Pataz gold field, northern Peru

W. K. Witt[a], S. G. Hagemann[a], J. Ojala[b], C. Laukamp[c], T. Vennemann[d], C. Villanes[e] & V. Nykanen[f]

[a] Centre for Exploration Targeting, University of Western Australia, WA 6009, Australia.

[b] Store North Gull AS, PO Box 613, 971, Longyearbyen, Norway.

[c] CSIRO Earth Science and Resource Engineering, 26 Dick Perry Avenue, Kensington, WA 6151, Australia.

[d] University of Lausanne, CH-1015, Lausanne, Switzerland.

[e] Compania Minera Poderosa S.A., Av Primavera 834, Surco, Lima-33, Peru.

[f] Geological Survey of Finland, PO Box 77, FI-96101, Rovaneimi, Finland.

Published online: 23 Apr 2013.

To cite this article: W. K. Witt, S. G. Hagemann, J. Ojala, C. Laukamp, T. Vennemann, C. Villanes & V. Nykanen (2014) Multiple methods for regional- to mine-scale targeting, Pataz gold field, northern Peru, Australian Journal of Earth Sciences: An International Geoscience Journal of the Geological Society of Australia, 61:1, 43-58, DOI: 10.1080/08120099.2013.763859

To link to this article: http://dx.doi.org/10.1080/08120099.2013.763859

Australian Journal of Earth Sciences (2014)
61, 43–58, http://dx.doi.org/10.1080/08120099.2013.763859

Multiple methods for regional- to mine-scale targeting, Pataz gold field, northern Peru

W. K. WITT[1]*, S. G. HAGEMANN[1], J. OJALA[2], C. LAUKAMP[3], T. VENNEMANN[4], C. VILLANES[5] and V. NYKANEN[6]

[1]*Centre for Exploration Targeting, University of Western Australia, WA 6009, Australia.*
[2]*Store North Gull AS, PO Box 613, 971, Longyearbyen, Norway.*
[3]*CSIRO Earth Science and Resource Engineering, 26 Dick Perry Avenue, Kensington, WA 6151, Australia.*
[4]*University of Lausanne, CH-1015, Lausanne, Switzerland.*
[5]*Compania Minera Poderosa S.A., Av Primavera 834, Surco, Lima-33, Peru.*
[6]*Geological Survey of Finland, PO Box 77, FI-96101, Rovaneimi, Finland.*

Gold production in the Pataz district, northern Peru, is derived from mesothermal veins hosted by the Pataz batholith and basement-hosted epithermal and carbonate–base metal veins. At the regional scale, processing of Advanced Spaceborne Thermal Emission and Reflection Radiometer data can be used to delineate district-scale argillic alteration. One such area extends for tens of kilometres NNW of Vijus in the Maranon Valley. At the southern end of this area, basement-hosted quartz–carbonate–sulfide veins in faults support artisanal gold-mining operations. SEM analyses show that the alteration envelopes around these faults are dominated by illitic clays. These artisanal gold workings highlight the economic potential of the largely unexplored parts of the district-scale argillic alteration zone, further north. At the district scale, paleostress modelling maps areas of low minimum stress during Carboniferous ENE–WSW shortening, based on a new 1:25 000 geological map of the Pataz district. The resulting distribution of low minimum stress is used to predict sites of rock fracture under high fluid pressure, and consequent vein formation. These areas of low minimum stress occupy 11% of the modelled area but contain 50% of the known veins in the Pataz district. Some areas of low minimum stress contain no known veins, and where these are poorly explored or poorly exposed, they are proposed as potential targets for gold exploration. In combination with SEM microanalysis, ASD hyperspectral reflectance analysis of drill core samples shows that visible proximal sericitic alteration around batholith-hosted auriferous veins is predominantly phengitic illite. Automated software interpretation of ASD reflectance spectra using *The Spectral Assistant* shows that sericite in cryptic alteration distal from auriferous veins varies from mainly illite adjacent to the phengitic illite zone, to more distal muscovite. Reactivation of faults and mineralised vein contacts during the largely Cenozoic Andean orogeny produced chlorite alteration that locally overprints proximal phengitic illite alteration. ASD spectrometry identifies relict phengitic illite in some chloritic alteration zones and thus indicates proximity to mineralised veins at the deposit scale. Elevated pathfinder element concentrations within proximal phengitic illite alteration zones around batholith-hosted veins do not extend more than a few metres beyond the visible alteration envelope. The alkali alteration index $((Rb + Cs)/Th)_N$ is elevated above background levels for up to 15 m beyond the visible sericite alteration zone in one of two holes investigated. In the other hole, both $((Rb + Cs)/Th)_N$ and 3K/Al can be used as a lode-scale vector to gold-bearing veins within broad intersections of visible sericite alteration.

KEY WORDS: exploration targeting, gold, Peru, ASTER, spectral geology, stress modelling, geochemistry.

INTRODUCTION

The Pataz–Parcoy gold-mining area, in the Eastern Andean Cordillera of northern Peru (Figure 1), has produced more than 8 million ounces of gold, mostly from quartz–carbonate–sulfide veins in the Carboniferous (Mississippian) dioritic to monzogranitic Pataz batholith (Haeberlin *et al.* 2004; Compania Minera Poderosa S.A., unpublished data). In the Pataz district (the northern half of the Pataz–Parcoy gold-mining area), gold in batholith-hosted veins is mined by Compania Minera Poderosa S.A. (CMPSA), and extracted by artisanal miners from a number of small country rock-hosted mines and workings in the Vijus–Santa Filomena area (Figure 1). Most of these smaller mines are hosted by the basement Maranon Complex, although there are also a few workings in sedimentary rocks of the Chagual Graben and in volcanic rocks of the Lavasen Graben (Figure 1).

*Corresponding author: wittww@iinet.net.au

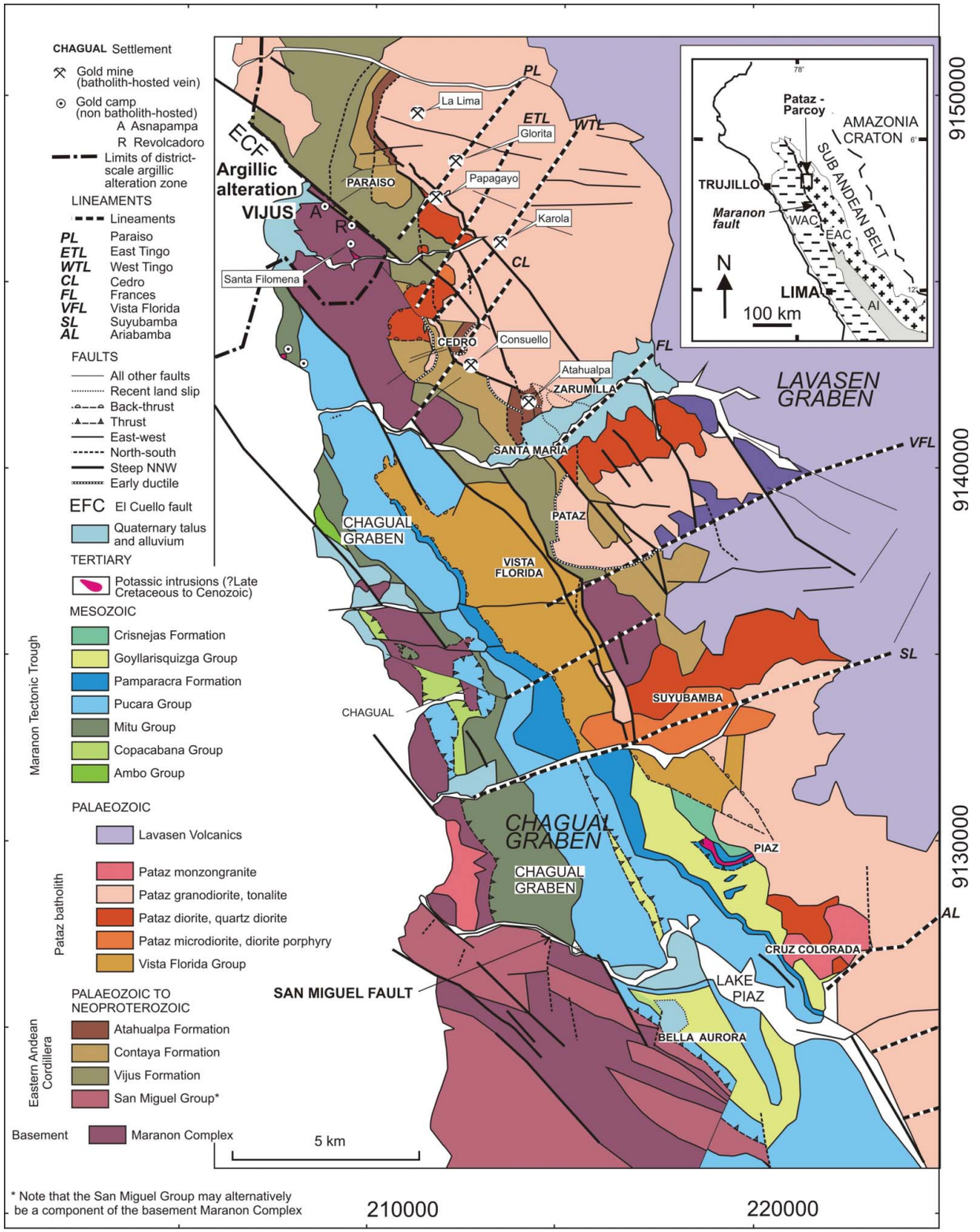

Figure 1 Geological map of the Pataz district, northern Peru, showing major, batholith-hosted gold mines and smaller, artisanal gold mines near Vijus. Inset map shows location of the Pataz–Parcoy area in the Eastern Andean Cordillera (EAC). Other abbreviations in the inset map are Western Andean Cordillera (WAC) and Altiplano and intermontaine basins (AI).

The classification of the batholith-hosted veins has been contentious. Early studies interpreted the veins as intrusion-related deposits linked with Mesozoic to Cenozoic monzonite to tonalite porphyries (Vidal *et al.* 1995) or calc-alkaline intrusions of the Pataz batholith (Schreiber *et al.* 1990a, b; Macfarlane *et al.* 1999). An orogenic model developed by Haeberlin *et al.* (2002, 2004) using ^{40}Ar–^{39}Ar geochronological data showed a 15 Ma

time gap between emplacement of the Pataz batholith (*ca* 328 Ma) and hydrothermal sericite from proximal alteration zones around mineralised veins (314–312 Ma). Witt *et al.* (2009) supported the orogenic classification of batholith-hosted veins in the Pataz district while suggesting a Cretaceous or Cenozoic epithermal model for mineralisation in the Maranon Complex and allochthonous sedimentary rocks in the Chagual Graben. Subsequent observations and data (including results of K–Ar dating of clays in the Vijus area) indicated that most of the gold-related hydrothermal alteration in the Pataz district is older than the Cretaceous and may possibly represent a single Carboniferous metallogenic event (Witt *et al.* 2011). Differential uplift during the late Carboniferous and Cenozoic juxtaposed mesothermal veins in the Pataz batholith against basement-hosted epithermal and carbonate-base metal veins (Witt *et al.* 2011). The relatively few known occurrences of gold mineralisation in the allochthonous sedimentary rocks of the Chagual Graben must be younger than the Late Cretaceous tectonic emplacement of the host rocks or have formed at an earlier time in the Western Andean Cordillera and have been tectonically transported into the Pataz district with their host rocks. They are not discussed in this paper.

Irrespective of the genetic classification of the batholith-hosted and basement-hosted auriferous veins, which remain enigmatic, this paper seeks to examine empirical exploration techniques that can be successfully applied to gold exploration in the Pataz district. The techniques considered have utility at different scales of exploration, and are described in terms of regional-, district- and deposit-scale targeting. They are, from regional-scale techniques to deposit-scale techniques: (1) Advanced Spaceborne Thermal Emission and Reflection Radiometer (ASTER) multispectral imagery, processed to identify and delineate areas of argillic alteration with associated gold mineralisation in the Chagual Graben; (2) paleostress modelling to determine areas of likely vein formation during the early Carboniferous (Mississippian); (3) ASD hyperspectral mineralogy for distinguishing between phyllosilicate minerals that are proximal and distal to the mineralised batholith-hosted veins; and (4) trace-element analyses of drill core to highlight the relationship between alkali element alteration indices and proximity to mineralised batholith-hosted veins.

GEOLOGY OF THE PATAZ DISTRICT AND GEOLOGICAL SETTING OF GOLD MINERALISATION

Pataz and Parcoy lie within the Maranon River valley, which follows an important NNW-striking morphological and tectonic lineament (the Cordillera Blanca Fault of Petford & Atherton 1992) in northern Peru, separating the Western and Eastern Andean Cordilleras (Figure 1 inset; Megard 1984; Schreiber *et al.* 1990b; Benavides-Caceres 1999). The geology of the Pataz district is essentially that of a horst and graben terrane characterised by major faults, geological contacts and the long axis of the Pataz batholith, all with a NNW trend (Figure 1). Although poorly exposed or expressed at the outcrop scale, NE- to ENE-trending structures coincident with prominent drainage lineaments are also important. Structures with these orientations have profound effects on the geology of the Pataz district, including segmentation of the Pataz batholith (Figure 1), and they probably acted as transfer faults during rifting.

The oldest rocks in the Pataz district belong to the latest Neoproterozoic to early Cambrian basement, termed the Maranon Complex, exposed near Vijus, on the western margin of a horst and, more broadly, on both sides of the Chagual Graben (Figure 1). The Maranon Complex comprises multiply deformed phyllite, mica schist and graphitic schist, metamorphosed to greenschist to lower amphibolite facies assemblages during the early to middle Cambrian Pampean orogeny (Haeberlin *et al.* 2004; Cawood 2005). The succession of volcanic and sedimentary units that defines the Eastern Andean Cordillera was deposited unconformably on the Maranon basement during the late Cambrian and Ordovician (Schreiber *et al.* 1990a; Haeberlin *et al.* 2004). The Mississippian Pataz batholith is a 60 km long, dioritic to monzogranitic composite intrusion that intruded units of the Eastern Andean Cordillera and is sub-parallel to the NNW structural grain (Figure 1). Robust LA-ICP-MS and SHRIMP U–Pb in zircon geochronology indicate emplacement of the batholith between *ca* 338 and 335 Ma (Miskovic *et al.* 2009; Witt *et al.* 2013). Felsic volcaniclastic rocks of the poorly studied Lavasen Formation are conventionally regarded as having been deposited during the Miocene to Pliocene (Wilson & Reyes 1997). However, recent results of U–Pb in zircon geochronological studies have shown that the Lavasen Volcanics in the Pataz district are Carboniferous and only a few million years younger than the Pataz batholith (A. Miskovic, pers. comm. December 2009; Witt *et al.* 2013).

The Carboniferous and older rocks were deformed during the Carboniferous Gondwanide orogeny (Schaltegger *et al.* 2006). The mineralised batholith-hosted veins formed during uplift at the end of the Gondwanide orogeny. Metasomatic sericite from the alteration halos around examples of these veins have been dated at 314–312 Ma, using $^{40}Ar/^{39}Ar$ techniques (Haeberlin *et al.* 2004), but these probably represent a minimum age of mineralisation (Witt *et al.* 2013). The Pataz district was subsequently deformed again during the Andean orogeny. In the early stages (Late Cretaceous) of this orogeny, sedimentary units deposited in the Maranon Tectonic Trough (in the Western Andean Cordillera) were thrust eastwards over older stratigraphic and intrusive units of the Eastern Andean Cordillera (Megard 1984; Macfarlane *et al.* 1999). Mostly removed by subsequent erosion, these sedimentary rocks are now preserved in the Chagual Graben (Figure 1), which formed during later stages of the Andean orogeny.

Much of the gold produced from the Pataz district has come from underground mines (Figure 1) that exploit metre-scale quartz–carbonate–sulfide veins along the western margin of the Pataz batholith. Sulfide minerals locally form up to 50 vol% of these veins and are predominantly pyrite and arsenopyrite, sphalerite and galena. Two main vein orientations (subhorizontal and moderately east-dipping) have been interpreted to result from regional ENE–WSW shortening (Haeberlin *et al.* 2004).

The veins are essentially brittle dilational structures associated with sericite alteration of the mainly granodiorite wallrocks. Although gold is anomalous in the sericite alteration zones, economic grades are generally confined to the veins. The structural effects of the Andean orogeny on batholith-hosted quartz–carbonate–sulfide veins are limited to minor buckling and local reorientation adjacent to major faults.

Gold mineralisation also occurs in the Vijus area where quartz–carbonate–sulfide (±barite, adularia, fluorite) veins are hosted by the Maranon Complex and are spatially related to the El Cuello Fault (ECF in Figure 1). Witt *et al.* (2011) classified the mineralisation at Santa Filomena area as carbonate–base metal mineralisation, formed at intermediate crustal levels, between epithermal and porphyry environments (Corbett & Leach 1998). Additionally, there are several small artisanal mining operations in allochthonous sedimentary units in the Chagual Graben. One example, a few kilometres southeast of Vijus (Figure 1), comprises quartz–carbonate–sulfide (±adularia, fluorite) breccia. Similar adularia- and fluorite-bearing veins have been recognised in the Estrella porphyry (of uncertain age; Witt *et al.* 2013), which intrudes the Maranon Complex near Santa Filomena.

REGIONAL-SCALE TARGETING FOR GOLD: ASTER MULTISPECTRAL DATA

ASTER data are available over and beyond the area shown in Figure 1. ASTER captures high spatial resolution data in 14 bands, from visible to thermal infrared wavelengths. The short wave infrared (SWIR) region contains five bands that facilitate the mapping of groups of clays, and thus delineate areas of phyllic, argillic and propylitic hydrothermal alteration (e.g. Crosta *et al.* 2009). Identification of white mica and clay mineral groups is achieved by mapping the position and depth of characteristic absorption features, particularly the 'AlOH' feature located at around 2200 nm in phyllosilicates (Vedder & McDonald 1963; Rowan & Mars 2003). Our terminology in regard to white mica and clays in this section and the later section on ASD analysis of drill core samples follows that of Rieder *et al.* (1999) such that muscovite and phengite are true micas, in which cations in the interlayer sites (K, Na, Ca) total >1.85, whereas illitic clays are hydrated and therefore contain <1.85 (K + Na + Ca) in the interlayer site. Phengite is a solid solution series between muscovite, aluminoceladonite and celadonite, and differs from muscovite by incorporating more divalent ions (generally Fe^{2+}) by substitution for octahedral Al (Rieder *et al.* 1999). Sericite is used to describe fine-grained white mica and/or illitic clay where a more specific identification is not available.

In the Pataz district, ASTER imagery highlights a district-scale area of pervasive argillic alteration in basement schists of the Maranon Complex, which extends for almost 50 km in an NNW direction from Vijus (Figure 2). Between Vijus and Chicun, the alteration zone is up to several kilometres wide and coincides with the strike projection of the Maranon Complex basement horst. At the surface, this area contains sparse vegetation and appears bleached, reflecting the widespread abundance

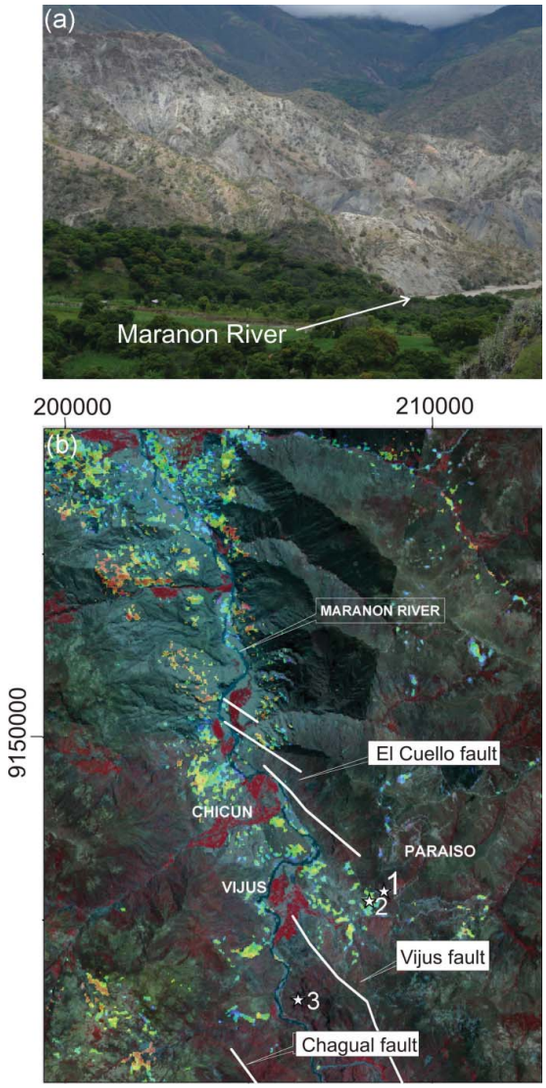

Figure 2 (a) Looking northwest across the Maranon River from Vijus showing the vegetation anomaly (white to pale grey 'badlands') in the foreground and darker (vegetated), less altered or weathered rocks in the background. (b) ASTER image showing varying location of 'AlOH' absorption feature (yellow to green = short wavelength–illite-rich; red to orange = long wavelength–phengite-rich; the deep red patches are vegetation anomalies). The major north northwest-striking faults are shown as well as gold deposits and prospects referred to in the text (1. Santa Filomena, 2. Estrella, 3. Vijus breccia).

of clay minerals (Figure 2a). ASTER imagery highlights an abundance anomaly for AlOH-bearing phyllosilicates, such as white micas, kaolinite and aluminosmectites. The AlOH abundance anomalies also occur in major streams that drain the Lavasen Volcanics (e.g. in the northeast corner of Figure 2b), where weak argillic alteration is widespread.

Outcropping schists of the Maranon Complex in the argillic alteration zone are friable and pale coloured, compared with unaltered basement schists exposed south of Chagual (Figure 1). On the basis of ASTER data processed to identify the location and depth of the 'AlOH'

absorption feature, the alteration zone can be subdivided into short AlOH wavelength and long AlOH wavelength domains (Figure 2b). White micas and/or clays in the short-wavelength domains are likely to be dominated by muscovite or kaolin. White mica in long-wavelength domains are Al-poor and likely to be more phengitic. No systematic pattern of zoning is recognised between short-wavelength and long-wavelength domains. Seven grab samples of altered schist taken from the district-scale zone of pervasive argillic alteration, between Chicun and Santa Filomena, were analysed by XRD at AMDEL Laboratories, Adelaide, South Australia, and results show that the samples are predominantly composed of quartz, albite and 'mica' with relatively minor amounts of chlorite and K-feldspar and, locally, kaolinite (Supplementary Papers Table 1). The XRD analysis reports 'mica', but this description covers a wide range of clays as well as white micas.

The area north of Chicun is poorly explored owing to competing land uses, but at the southern end of the argillic alteration zone, gold–base metal mineralisation occurs at Asnapampa, Revolcadoro, Santa Filomena, Estrella and south of Vijus (Figures 1, 2b). In these areas, clays are further concentrated in centimetre- to metre-scale argillic alteration halos around numerous brittle faults between the larger-scale El Cuello and Vijus faults. Several of these faults contain quartz–carbonate (ankerite, siderite)–sulfide (pyrite, arsenopyrite, sphalerite, galena) veins that carry sufficient gold to support artisanal mining. The most advanced of these prospects is at Santa Filomena where a 1000 m long, complex, branching, E–W fault contains a centimetre- to metre-scale quartz–carbonate–sulfide (±barite) vein. Additionally, barren steeply dipping carbonate (calcite, ankerite, siderite) and sulfate (barite) veins are fairly widespread within the Vijus–Santa Filomena area.

The XRD analyses and petrographic observations show that samples collected from surface exposures of these faults are dominated by quartz, iron oxides and 'mica' (Supplementary Papers Table 1), with barite and traces of pyrite or sphalerite in some samples. Iron oxides replace iron-bearing carbonate minerals and sulfides. Feldspars are largely destroyed by hydrothermal alteration and replaced by clays. Clay minerals associated with gold and base metal mineralisation at Santa Filomena and Asnapampa have been analysed by SEM (scanning electron microscope with quantitative EDAX-ray microanalysis capability), at the Centre for Microscopy, Characterisation and Analysis, University of Western Australia. Results presented in Figure 3 and Supplementary Papers Table 2 show that the 'mica' identified by XRD is predominantly illitic clay with compositions intermediate between hydromuscovite and illite. At Asnapampa, illitic clay is interleaved with chlorite and pale yellow kaolin. The contrasting trends shown by data from Santa Filomena and that from Asnapampa (Figure 3) are possibly the result of weathering in samples taken from near surface workings at Asnapampa.

Illitic clay has been separated from samples representing argillic alteration and analysed for oxygen and hydrogen isotopes at the University of Lausanne, Switzerland. Measurements of the hydrogen isotope compositions of clays were made using high-temperature (1450°C) reduction methods with He-carrier gas and a TC-EA linked to a Delta Plus XL mass spectrometer from Thermo-Finnigan on 2–4 mg sized samples according to a method adapted after Sharp *et al.* (2001). The oxygen isotope composition (^{16}O, ^{18}O) of the clay samples was measured at the University of Lausanne, using a method similar to that described by Sharp (1990) and Rumble & Hoering (1994), described in more detail in Kasemann *et al.* (2001). The analytical results (Figure 4), assuming geologically reasonable temperatures for argillic alteration (100–200°C), indicate that the district-scale alteration between Chicun and Vijus was caused by a predominantly magmatic hydrothermal fluid, and that this magmatic signature has apparently been preserved despite exposure to weathering, probably since differential uplift during the Cenozoic Andean orogeny. The more intense argillic alteration halos around mineralised faults at Santa Filomena and Asnapampa were caused by magmatic hydrothermal fluid,

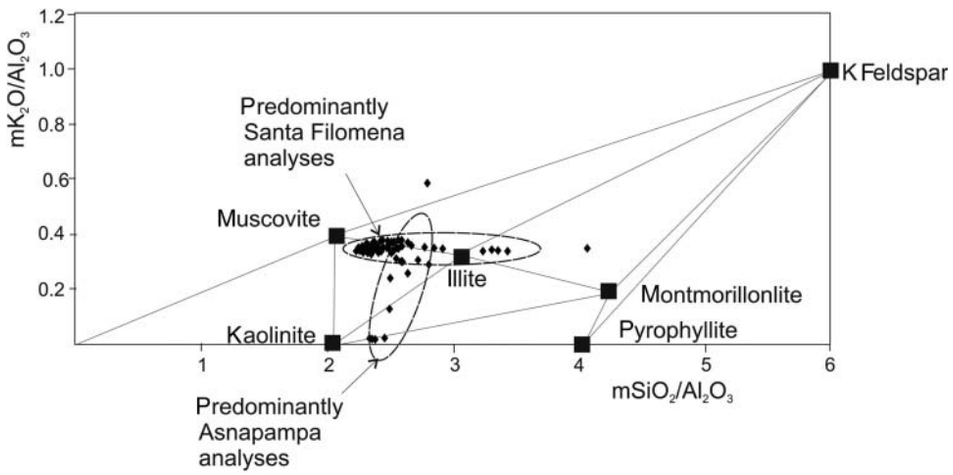

Figure 3 Garrels (1984) plot of sericite analyses from Santa Filomena and Asnampampa. Analyses conducted using an SEM with EDAX facility, using current of 3 nA and voltage of 15 kV and a run time of 60 s.

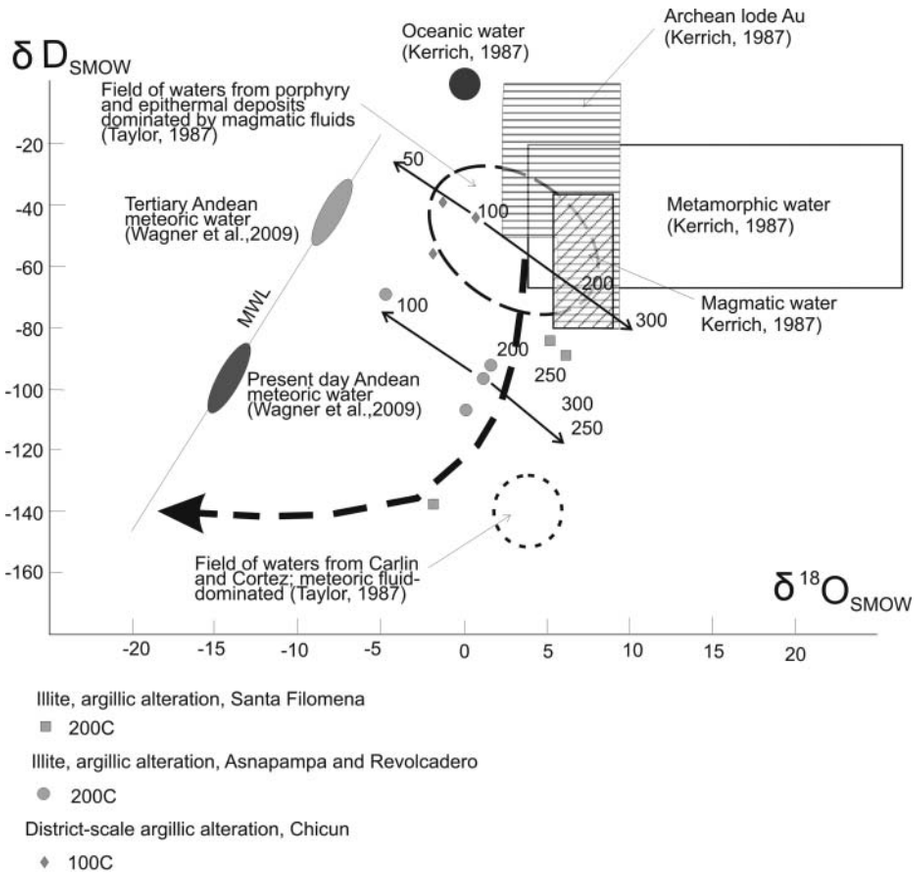

Figure 4 Plot of δD *vs* δ^{18}O for clay separates taken from the district-scale argillic alteration zone NNW of Vijus, from near-surface workings in the Asnapampa and Revolcadoro areas and from drill core at Santa Filomena. Temperatures of alteration are unknown but estimated based on geologically comparable zones of near-surface argillic alteration (~100°C, Hedenquist *et al.* 2000) and carbonate–base metal veins (~200°C; Richards *et al.* 1997). Generalised trends of variations in isotopic values with temperature are shown as arrows annotated with numbers (i.e. temperature, °C) to illustrate the effects of an incorrect temperature assumption. The J-shaped broken line curve is a generalised form of water/rock equilibration at ratios between 0 and 100 (from Taylor 1977). The curve links fluids dominated by magmatic fluids (Taylor 1987) with a hypothetical Carboniferous meteoric fluid characterised by δD = –140‰ and δ^{18}O = –20‰.

but the hydrothermally altered rocks have partially equilibrated with isotopically depleted (?Carboniferous) meteoric water.

DISTRICT-SCALE TARGETING FOR GOLD: PALEOSTRESS MAPPING

Paleostress mapping is a geomechanical modelling technique developed to target epigenetic mineralisation located in dilatant (low stress) sites (Holyland & Ojala 1997). The paleostress model utilises the distinct element method (UDEC program, Itasca Consulting Group), which is a recognised discontinuum modelling approach for simulating the behaviour of jointed rock masses. Applied to gold exploration, the technique is based on the premise that gold deposits form in sites of focused fluid flow, and these in turn are equivalent to areas of low minimum principal stress. The numerical modelling method seeks to transform strain data, in the form of a solid geology map, to stress data, using the principles of rock mechanics, including stress–strain relationships. Geological mapping in the Pataz district has shown that Cenozoic Andean orogenic overprinting of Carboniferous mineralisation has been partitioned into suitably oriented faults. Geological units and batholith-hosted veins, which lie outside fault zones, have not been significantly redistributed during the Andean orogeny, although some veins are locally reoriented adjacent to faults (Witt *et al.* 2009).

The geological map utilised for 2D stress modelling was based on a 1:25 000 scale map of the Pataz district produced by the senior author in 2009–2010. For geomechanical modelling, discontinuities (faults and contacts) were extrapolated to form a polygonal network. In order for the map to be useful for the purposes of stress modelling, the geology had to be projected to a constant elevation (2000 m asl in this case) and further modified to discount the effects of post-mineralisation events. These included tectonic emplacement of the allochthonous sedimentary units and formation of the Chagual Graben. The resulting map, shown in Figure 5a, shows a thin NNW-striking strip of sedimentary and volcaniclastic rocks (Eastern Andean Cordillera) separating the segmented Pataz batholith from the Maranon Complex (basement). Two smaller granite bodies intrude the Maranon Complex and the Vijus Formation (Eastern Andean Cordillera). The area is traversed by a network of faults and fractures, the most prominent sets being oriented NW to NNW and NE to ENE. Compania Minera Poderosa S.A. (CMPSA) provided digital GIS data identifying the distribution of known quartz veins in the Pataz district (Figure 5).

Our initial models assumed that the age of the Lavasen Volcanics is Cenozoic, following Wilson & Reyes (1997), and this unit was also removed for modelling purposes. Stress was simulated using an ENE–WSW far-field shortening direction, consistent with the conclusions of Haeberlin *et al.* (2004) and with our own observations

(Witt *et al.* 2009). Subsequent geochronological investigations (A. Miskovic, pers. comm.; Witt *et al.* 2013) have shown that the Lavasen Volcanics are Carboniferous (between 336 and 330 Ma). Therefore, a second model retains the Lavasen Volcanics as a thick pile of felsic volcaniclastic rocks in the Lavasen Graben to the east of the Pataz batholith (Figure 5c). A shortening direction of ENE–WSW was also employed for this second model.

The results of the UDEC modelling are shown in Figure 5(b, d) and Supplementary Papers Table 3, where areas in blue have the lowest minimum principal stress, and areas in yellow to red have a higher minimum principal stress. Sites of low minimum principal stress are most likely to be dilatant, and the first to fracture, under applied stress and are theoretically potential sites of vein formation under high fluid pressure and focused fluid flow. Zones of fracturing caused by a dilation of rock volume are also sites of focused hydrothermal fluid flow and are, therefore, potential targets for gold exploration.

A measure of the success of the modelling is the degree of coincidence between low minimum principal stress sites obtained from the modelling and known auriferous veins as defined by geological mapping and exploration drilling. Where the Lavasen Volcanics are not included in the ENE–WSW shortening model, low stress areas over about 10% of the model area contain 43% of the quartz veins (Supplementary Papers Table 3). The results of stress modelling for the model incorporating Lavasen Volcanics are similar to those without Lavasen Volcanics, but low minimum stress sites are more extensive, especially along the faulted eastern margin of the Pataz batholith (Figure 5d). In the model that includes Lavasen Volcanics, low minimum stress areas occupy 11% of the total model area and contain 50% of the known quartz veins (Supplementary Papers Table 3).

These figures clearly indicate that the modelling results are not random, and that the geological map (Figure 1) and geomechanical (UDEC) model are reasonable interpretations of the Pataz district at the time of mineralisation. They show that paleostress modelling using the parameters chosen for the Pataz district has predictive capacity for the location of gold-bearing quartz–carbonate–sulfide veins. The results show that veins occurring in areas modelled as areas of low minimum stress are five times more abundant than a random distribution of veins would provide. These results also support the contention that the location and orientation of mineralised veins has not been significantly modified by tectonic events during the Late Cretaceous and Cenozoic Andean orogeny because significant post-mineralisation redistribution of the veins would tend to mask the relationships between vein distribution and the Carboniferous low minimum stress domains.

Inclusion of Lavasen Volcanics into the UDEC model has a relatively small effect on the distribution of veins with respect to low minimum stress domains (Figure 5b, d). However, inclusion of the Lavasen Volcanics at the time of gold mineralisation might have additional implications if the volcanics extended beyond the Lavasen Graben (Figure 1) and formed a thin layer over the Pataz batholith. A thin, hot volcanic layer such as this would potentially have acted as a mechanical and thermal seal, resistant to fracturing and the upward flow of fluids. As a result, such a seal would likely promote high fluid pressures and fracturing in the underlying batholith. This aspect of the genesis of the gold deposits has not been modelled.

DEPOSIT-SCALE TARGETING FOR GOLD: PHYLLOSILICATE MINERALOGY

The ASD hyperspectral analysis of rock samples was carried out using a TerraSpec Portable Vis/NIR instrument (Analytical Spectral Devices Inc.), by Scott Halley of Mineral Mapping Limited. The ASD analysis can be used to measure the abundance and composition of minerals with hydroxyl bonds, as well as carbonates or sulfates, and is therefore useful in the study of hydrothermal alteration. The TerraSpec instrument operates in the visible-, near- and short-wave infrared region, between 350 and 2500 nm. Characteristic reflectance spectra allow the identification of mineral species, as well as variations in the compositions of white micas and clays, based on the wavelength position of the 'AlOH' absorption feature located at around 2200 nm in phyllosilicate minerals. Shifts in the wavelength position of the AlOH feature are related to the Tschermaks exchange ($Al^{VI}Al^{IV}(Fe,Mg)_{-1}Si_{-1}$), where an increase in the wavelength position is correlated with an increase in the Si/Al ratio. A number of studies described the change in Al-content in phyllosilicate minerals from distal to proximal hydrothermal alteration associated with epithermal deposits (Carillo-Rosúa *et al.* 2009; Sonntag *et al.* 2012). Reflectance spectra were interpreted using The Spectral Assistant (TSA, a method built in to the software package The Spectral Geologist^{TM}), which matches the reflectance spectra of the sample mineral spectra to a reference mineral spectrum or a weighted combination of spectra for two minerals (Berman *et al.* 1999).

Core samples for ASD analysis were taken at spaced intervals through diamond cores SJX08-22, 15X08-123 and 38X08-450 from batholith-hosted veins in the Papagayo mine (Figure 1). The samples were closely spaced (0.5–1 m) close to the vein and progressively wider-spaced with distance from the vein (up to 10 m at distances >30 m). This strategy sampled the metre-scale proximal alteration and more distal cryptic alteration. Cryptic alteration is the pervasive, partial (possibly deuteric) alteration of feldspar to sericite that is not visually evident in the field. Results for the three holes that intersected batholith-hosted veins are shown in Figure 6. In all three holes, the host rock is granodiorite, thus eliminating host rock composition as a variable in the alteration mineralogy. Without the benefit of ASD reflectance data, visible hydrothermal alteration was logged as tens of centimetres to metres of proximal sericite alteration around mineralised veins. Metasomatic chlorite was less consistently present but mostly occurred in more distal positions.

For all three batholith-hosted holes, the characteristic wavelength position of the AlOH absorption feature for sericite in the proximal hydrothermal alteration zone is significantly greater than 2200 nm, and the mineral is

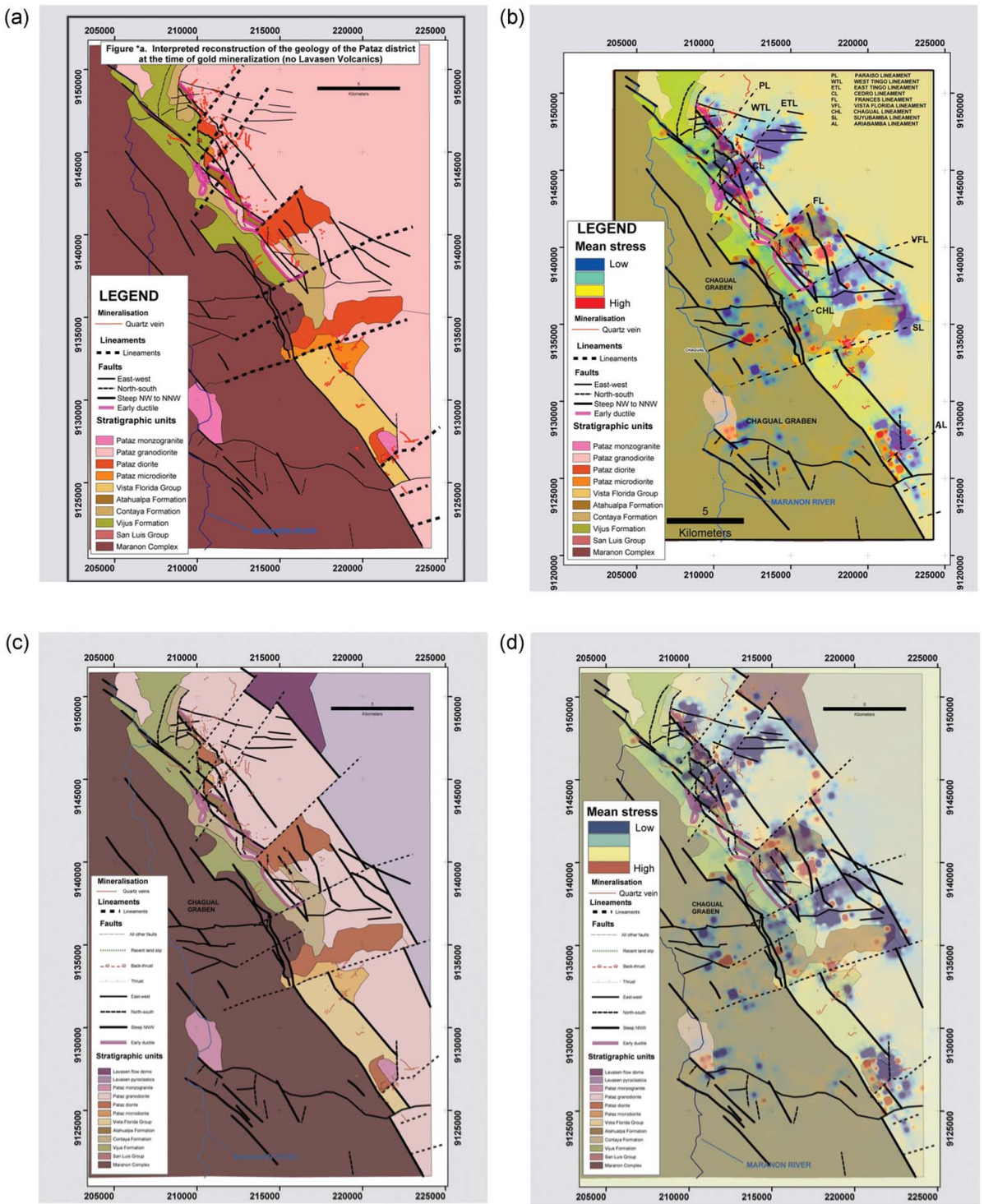

Figure 5 Results of stress modelling for the Pataz district, based on an ENE–WSW far field stress orientation during the Carboniferous. (a) Interpreted geology during the Carboniferous (assuming a Cenozoic age for the Lavasen Volcanics). (b) Distribution of minimum principal stress after application of far field stress. (c) Interpreted geology during the Carboniferous (assuming a Carboniferous age for the Lavasen Volcanics). (d) Distribution of minimum principal stress after application of far field stress. In b and d, blue areas represent lowest minimum principal stress and yellow to red areas represent higher minimum principal stress.

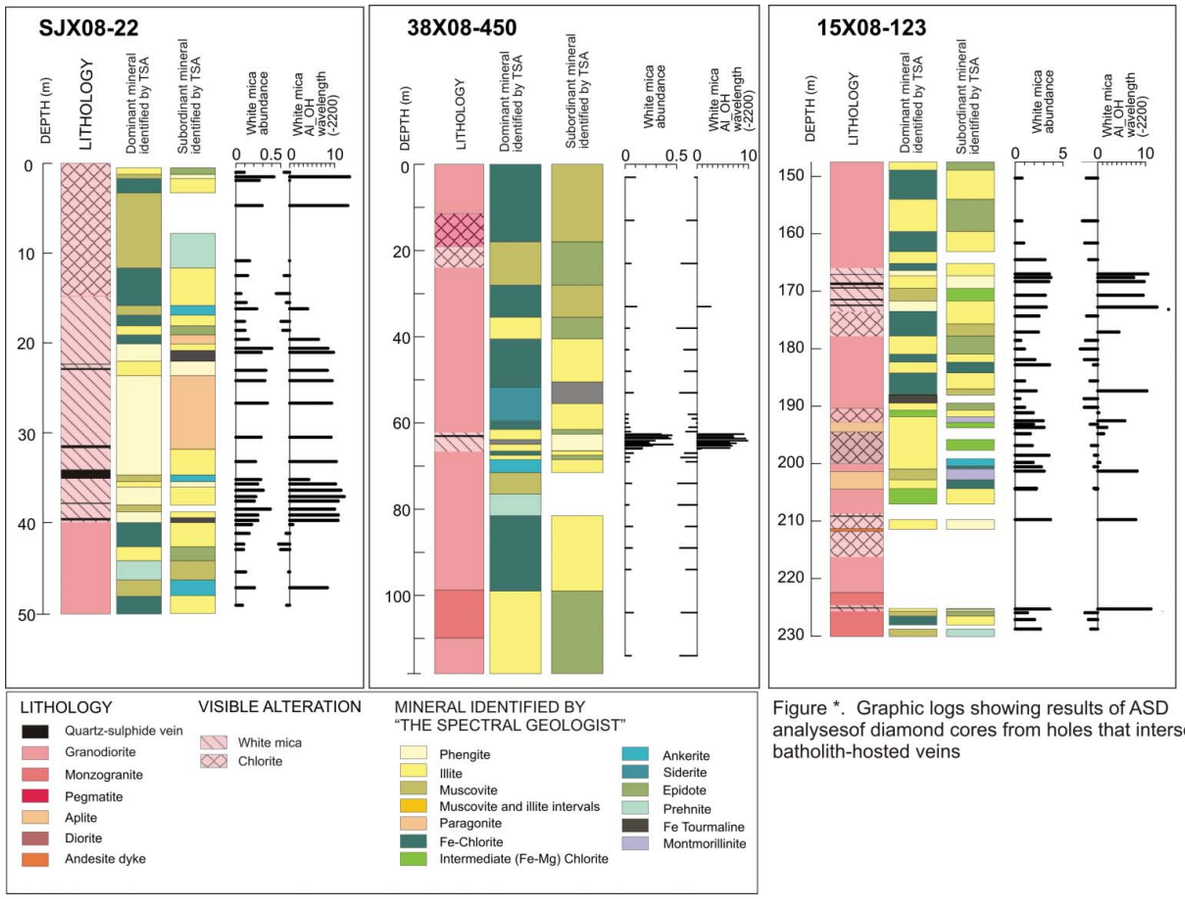

Figure *. Graphic logs showing results of ASD analysesof diamond cores from holes that intersected batholith-hosted veins

Figure 6 Graphic logs showing results of ASD analyses of diamond cores from holes that intersected batholith-hosted veins. Columns from left to right describe: (a) depth; (b) lithology and visible alteration as mapped by senior author (WW); (c) dominant mineral identified by TSA from the short wave infrared wavelengths (i.e. 'Min1 TSAS'); (d) subdominant mineral identified by TSA from the short wave infrared wavelengths (i.e. 'Min2 TSAS'); (e) white mica abundance derived from the absorption feature located at around 2200 nm, which is diagnostic for Al-bearing phyllosilicates (Values describe the relative depth of the diagnostic absorption feature after removal of the hull—the background or 'noise' component of the spectra.); and (f) wavelength position of the absorption feature located at around 2200 nm. Zero value equals 2200 nm and values below and above indicate shift to shorter (Al-rich white mica) and longer (Al-poor) wavelengths, respectively.

reported as phengite by The Spectral Assistant. SEM analyses (scanning electron microscope with quantitative ED X-ray microanalysis capability) carried out at the Centre for Microscopy, Characterisation and Analysis, University of Western Australia show that sericite in the proximal alteration zones range from hydromuscovite to illitic clays (Figure 7; Supplementary Papers Table 4), similar to those at Santa Filomena (Figure 3). Distal white mica is identified as illite or muscovite by The Spectral Assistant, both relatively Al-rich minerals with the characteristic spectral wavelength signature below or only slightly greater than 2200 nm. Muscovite appears to be distal with respect to illite in all three holes. Distal illite and muscovite are low in abundance; they were not identified as a visible alteration zone and probably are predominantly fine-grained white mica in feldspars, consistent with petrographic observations. These distal micas have not been analysed by SEM.

Visible chlorite alteration zones are rarely developed symmetrically around mineralised veins and proximal phengite alteration (Figure 6). Instead, visible chlorite alteration zones are either developed asymmetrically, on one side of the mineralised vein (SJX08-22 and 15X08-123) or are apparently unrelated to mineralised veins (15X08-123 and 38X08-450). Beyond visible chlorite alteration zones, cryptic alteration is characterised by alternating zones of minor Fe-chlorite and minor illite or muscovite (Figure 6). The ASD spectral analyses identify an Fe-rich variety of chlorite and also show that muscovite or illite is commonly present in visible chlorite alteration zones. Furthermore, in the deeper part of diamond hole 15X08-123, ASD analysis identified the presence of phengite within a visible chlorite alteration zone around a small quartz–carbonate–sulfide vein.

In summary, the combined application of conventional logging, SEM mineral analyses and ASD spectral reflectance technology has shown that hydrothermal alteration around mineralised veins in the Pataz batholith is zoned from proximal zones of visible illite with phengitic composition through relatively distal cryptic (?deuteric) illite and muscovite alteration zones.

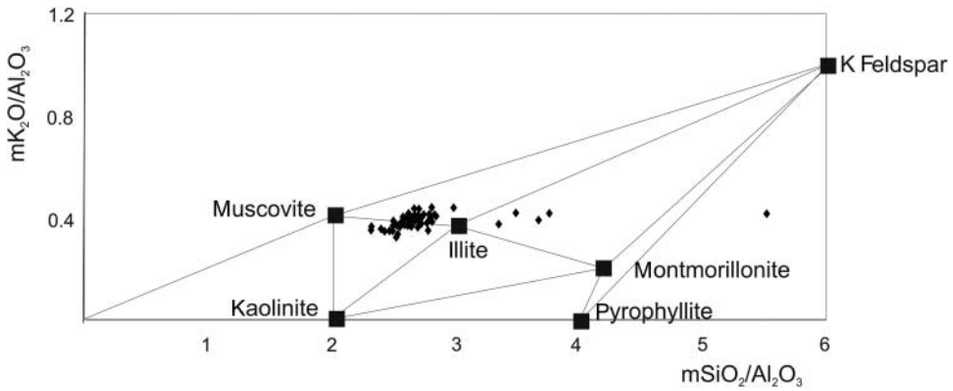

Figure 7 Garrels (1984) plot of sericite analyses from proximal alteration zones around batholith-hosted quartz–carbonate–sulfide veins, Papagayo, Glorita and Consuelo mines. Analyses conducted using an SEM with EDAX facility, using current of 3 nA and voltage of 15 kV and a run time of 60 s.

Although chlorite alteration is commonly developed as distal alteration with respect to proximal white mica in orogenic vein deposits (Witt 1993; McCuaig & Kerrich 1998), at Pataz the distribution of chlorite is less uniform (Figure 6). These observations, in combination with petrographic and underground mine observations, suggest that chlorite in the Pataz batholith formed during post-mineralisation reactivation of vein margins and other structural discontinuities in the batholith, most probably during the Andean orogeny.

These results suggest that ASD spectral analysis can be used as a vector towards mineralised batholith-hosted veins in some situations where visible alteration may not be as useful. For example, the presence of illite in cryptic alteration beyond zones of visible phengitic alteration suggests a more proximal environment compared with cryptic alteration zones characterised by muscovite. Similarly, visible chlorite alteration zones with a component of phengite or illite imply a more proximal environment compared with those that contain muscovite. Where visible phengitic alteration is intersected by exploration drilling, a mineralised vein should be anticipated within a few metres, providing the vein and its alteration halo have not been separated by post-mineralisation deformation.

LODE-SCALE TARGETING FOR GOLD: PATHFINDER ELEMENTS AND ALTERATION INDICES

Major and trace element geochemical analyses of diamond drill core were used to investigate the potential for geochemical dispersion as an exploration vector towards gold-bearing veins at the lode scale. Two diamond holes that intersected mineralised quartz veins were sampled: DH55X09-433, which intersected the Atahualpa vein in the Atahualpa mine, and DH75K09-027, which intersected the San Francisco vein at Pataz (Figure 1). These intersections are atypical in that the lode intersections are packages of relatively thin (centimetre-scale) veins rather than the metre-scale veins that are typically mined. However, these were the only cores available at the time of the study and are representative of the hydrothermal activity of the ore fluid that caused the batholith-hosted auriferous veins. Samples were taken at approximately 1 m intervals in the proximal alteration zone, expanding progressively to a spacing of 10 m at distances of 40 m from the ore zone. Sample spacing was modified slightly to avoid irregularities such as faults and dykes. The analytical suite comprised K_2O, Al_2O_3, Au, Ba, Ca, Cr, Cs, Cu, Fe, Li, Mg, Mn, Na, P, S, Sr, Ti, V, Zn, Zr, Ag, As, Be, Bi, Cd, Ce, Co, Hf, Ga, Ge, In, La, Lu, Mo, Nb, Pb, Rb, Sb, Sc, Se, Sn, Ta, Tb, Te, Th, Tl, U, W, Y and Yb.

A reconnaissance assessment of the multi-element data indicated that the most useful elements from an exploration perspective are Au, Cu, Pb, Bi, Mn, Sb, W, As, Te and Tl. In addition, the alkali alteration indices $(Rb + Cs/Th)_N$ (Heath & Campbell 2004) and 3K/Al (Kishida & Kerrich 1980) were assessed. Analyses were performed by SGS Laboratories Peru, by inductively coupled plasma mass spectrometry (ICM40B), except for gold, which was determined by fire assay (FAA313). Duplicate analyses indicate precision of better than 10% for gold at values >10 ppb; and better than 5% for Al, Cs, Cu, Mn, Rb, Sb, Th, Tl and W, and better than 10% for K, Pb, Bi and Te. Results of analyses of in-house laboratory standards indicate accuracy of better than 5% for Al and Cu, better than 10% for K, As and Pb and better than 20% for Mn. Other elements were either not represented by the in-house standards or gave poor accuracy owing to low concentrations in the standard. The critical point for this study, which does not compare results with external data, is the precision, because the study is based on relative abundances.

Down-hole plots of the more significant geochemical parameters are shown in Figures 8–11. For comparison, background values of pathfinder elements and elements used to calculate alteration indices have been established from analyses of eight least-altered granodiorite samples collected in the Pataz district for whole-rock geochemistry (Supplementary Papers Table 5). Whole-rock geochemical samples were analysed by Actlabs, Canada, using ICP for all elements except gold, As, Cs, Rb, Sb and Th, for which INAA was used. Duplicate analyses indicate precision of better than 5% for K, Al, Au, Cs, Cu, Mn, Rb, Sb, Th and W, and better than 10% for Pb and Bi. Results of analyses of certified international standards (NIST-64, DNC-1, BIR-1, GXR-4, GXR-2, SDC-1, SCO-1, GXR-6, FK-1, NIST-1633b, SY-2, W-2a, OREAS-13P,

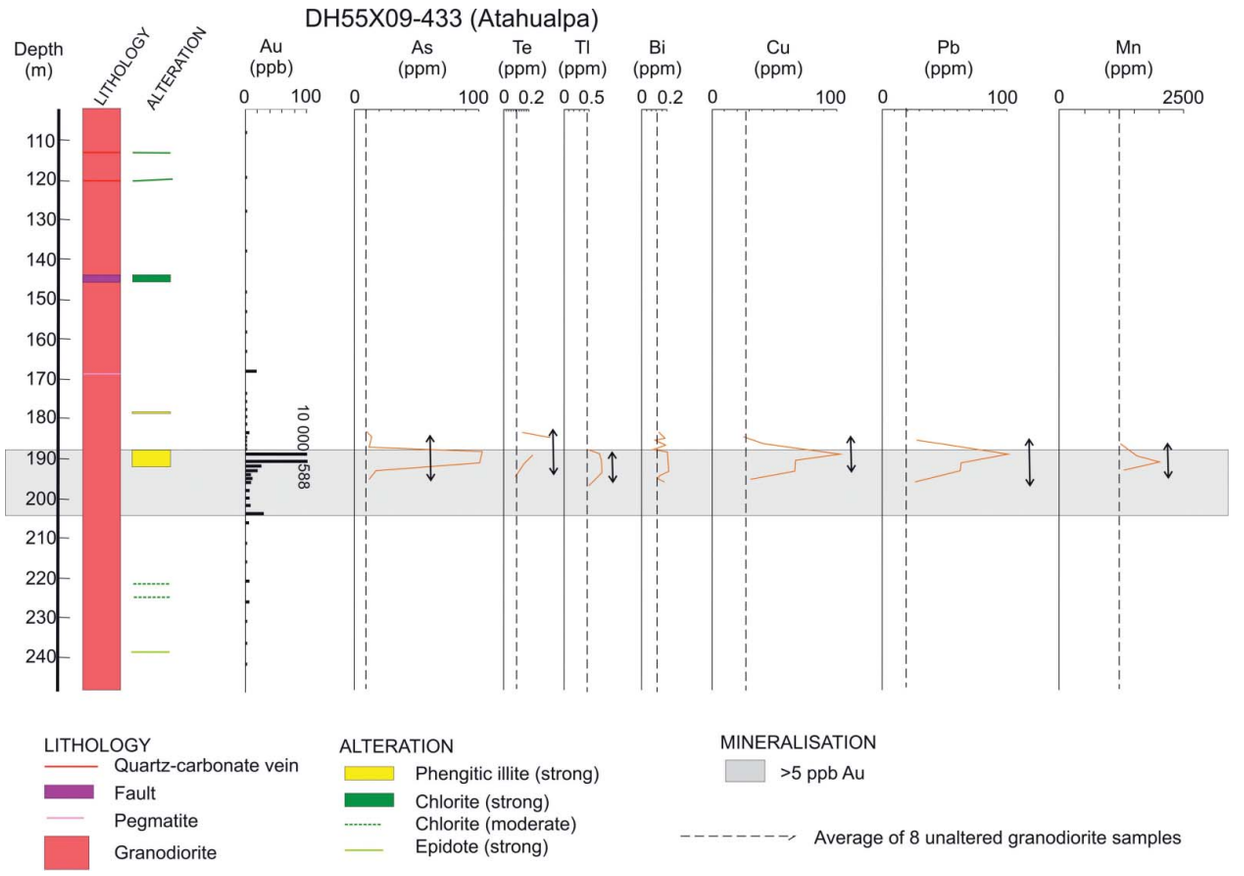

Figure 8 Strip log, drill hole DH55X09-433 (Atahualpa), showing geology, gold and pathfinder elements As, Te, Tl, Bi, Cu, Pb, Mn.

NIST-696, JSD-3) indicate accuracy better than 5% for K_2O, Al_2O_3, MnO, Pb and Rb, and better than 10% for most trace elements.

Drill hole DH55X09-433 (Atahualpa) intersected approximately 2.65 m of sericite (inferred phengitic hydromuscovite and illite on the basis of ASD and SEM analyses) alteration with up to 5 vol% disseminated sulfides (pyrite > arsenopyrite) within granodiorite, between 188.60 and 191.26 m (Figure 8). This interval includes approximately nine thin (≤5 cm) quartz–carbonate–sulfide (arsenopyrite ≫ pyrite) veins. Collectively, these veins represent the Atahualpa vein ore body at this location. The mineralised veins in this intersection are not laminated or breccia-textured but are zoned from sulfide-rich margins to quartz-rich cores, and are cut by later, milky white quartz veins. The best gold grades occur within the visible sericitic alteration zone, but gold values >5 ppb Au (the threshold of detection and local background) extend 11 m below it, in granodiorite with no visible alteration.

Drill hole DH75K09-027 (San Francisco) intersected a broad zone of moderate to strong chlorite and sericite (inferred phengitic illite on the basis of ASD and SEM analyses) alteration in granodiorite, within and beneath a prominent fault between 153 and 170 m (Figure 9). Hydrothermal alteration extends at least 116 m to the bottom of the hole at 269 m. Below 202 m, where sericitic alteration alternates with chloritic alteration, a broad zone of anomalous gold (>5 ppb Au) extends to the bottom of the hole. Sericite alteration zones within this interval contain 2–5 vol% disseminated pyrite and arsenopyrite, and centimetre-scale quartz–carbonate–sulfide veins. The zones of sericite alteration and veins generally coincide with better gold grades (>100 ppb Au).

Pathfinder elements

Among the pathfinder elements, As, Te, Tl, Bi, Cu, Pb and Mn display moderate to strong enrichment (over average unaltered granodiorite values) in most zones of elevated gold grade (Au > 100 ppb), in both holes (Figures 8, 9). Enrichment of Mn most likely reflects the composition and abundance of hydrothermal carbonate minerals whereas the other pathfinder elements are probably found as major or trace components of sulfide minerals. In DH55X09-433 (Atahualpa), some of these anomalies extend a few metres into the hanging wall of the ore zone and the associated visible sericite alteration (Figure 8). However, anomalism does not extend beyond the anomalous gold interval (>5 ppb Au) in the footwall. At San Francisco, some anomalous pathfinder element intervals (As, Tl, Bi, Cu, Mn) extend a few metres beyond sericite alteration zones into the adjacent chloritic alteration zones (Figure 9). Of these, As, Bi, Cu and Mn extend

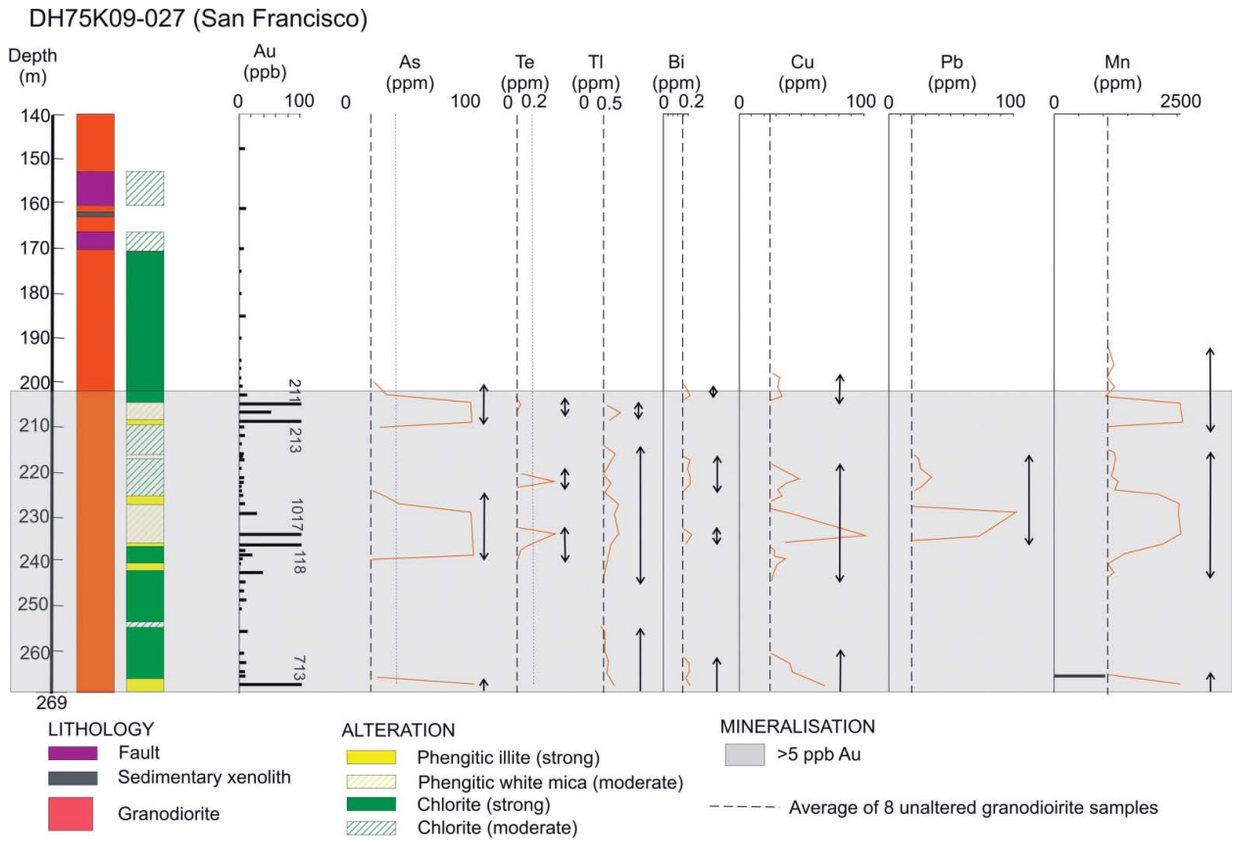

Figure 9 Strip log, drilll hole DH75K09-027 (San Francisco), showing geology, gold and pathfinder elements As, Te, Tl, Bi, Cu, Pb, Mn.

up to a few metres into the hanging wall, above the sericite alteration zone and beyond the anomalous gold interval.

Pathfinder-element anomalies appear to have limited application for mine-scale exploration because anomalous values do not extend more than a few metres beyond the visible white mica alteration zones and the anomalous gold zone. However, some pathfinder elements (As, Tl, Cu and Mn) provide potential vectors to mineralisation (>100 ppb Au) within broad areas of alteration and low-grade gold. This is illustrated by San Francisco hole DH75K09-027, where these elements remain anomalous for several to 10 m beyond the ore grade zone at 235 m.

Alkali index ratios

Down-hole variations in $(Rb + Cs/Th)_N$ and 3K/Al through DH55X09-433 (Atahualpa) and DH75X09-027 (San Francisco) are shown in Figures 10 and 11, respectively. The $(Rb + Cs/Th)_N$ values are compared with a background value of 1.6 (average for eight whole-rock analyses of least-altered granodiorite) and a mean value of 2.1 or 2.8 (average of all values in the respective drill hole). This ratio reflects the substitution of Rb and Cs for K in metasomatic micas (Heath & Campbell 2004). The 3K/Al values are similarly compared with a background value of 0.5 and a mean value of 0.5 or 0.45. This ratio reflects the extent to which Al in the host rock combines with K to form metasomatic white mica (Kishida & Kerrich 1987).

Both indices are elevated well above mean values within the ore zone (>100 ppb Au) in the hole from Atahualpa (Figure 10). Although erratic, where closely spaced sampling has taken place, $(Rb + Cs/Th)_N$ values above the mean are common in an interval (shown with double-headed arrow in Figure 10) extending beyond the visible white mica alteration zone and even 5 to 10 m beyond the anomalous gold zone (>5 ppb Au). The erratic nature of the index in the anomalous gold zone may be related to late-stage, barren, milky white quartz veins that overprint the mineralised veins. Although only wallrock was sampled, the late and barren hydrothermal event may have partially destroyed the $(Rb + Cs/Th)_N$ patterns related to the auriferous hydrothermal event through destruction of K (Rb, Cs) phyllosilicate minerals. Beyond the interval represented by the double-headed arrow, $(Rb + Cs/Th)_N$ values decrease to background levels over distances of about 20 m, before increasing again. It is not known if these distal increases of $(Rb + Cs/Th)_N$ indicate proximity to other zones of sericite alteration (±gold mineralisation) not intersected by the drill hole, but the laminated quartz–carbonate veins associated with disseminated pyrrhotite, between 110 and 120 m, suggest that this may be the cause. In any case, it appears that $(Rb + Cs/Th)_N$ appears to be enriched above

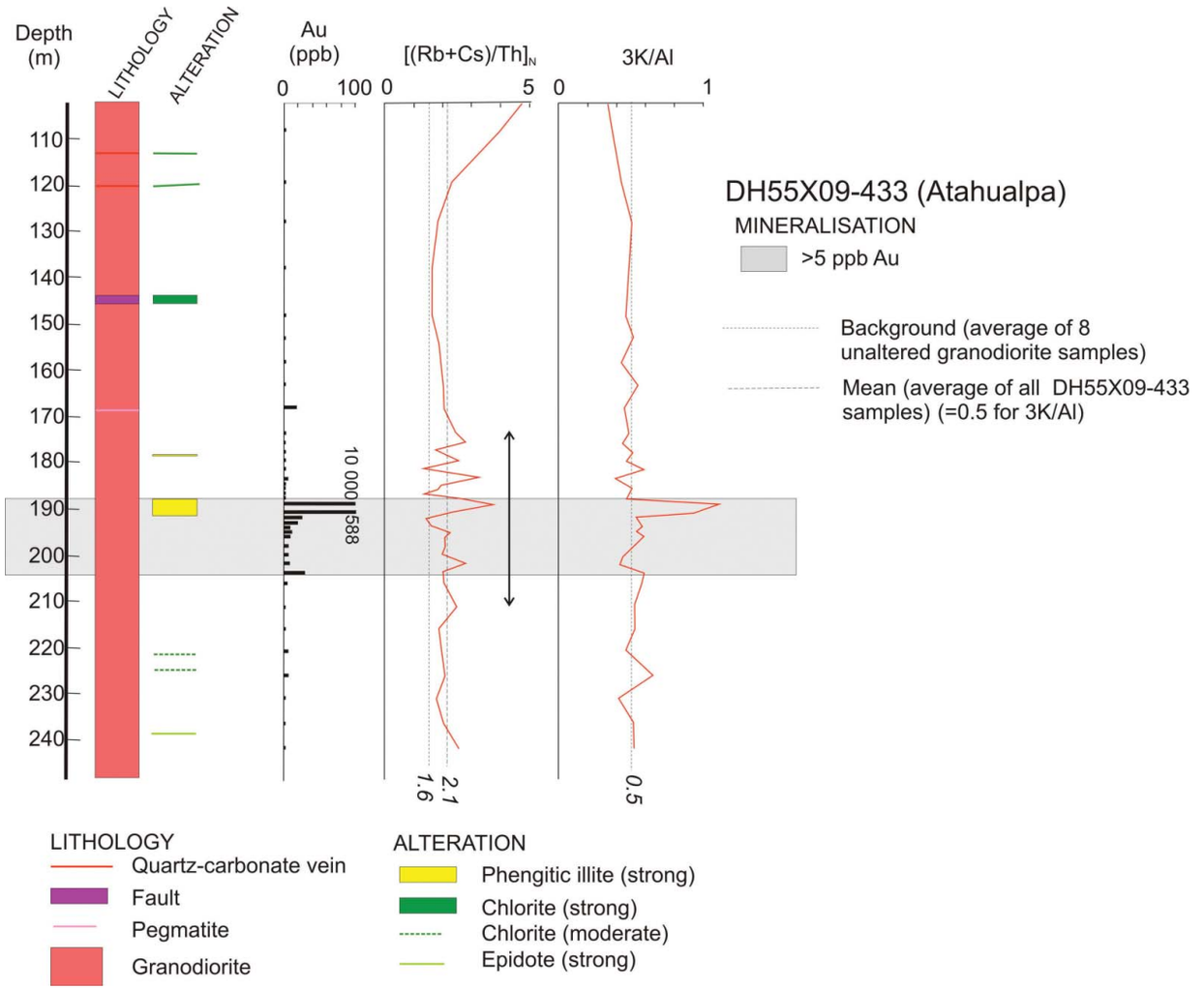

Figure 10 Strip log, drill hole DH55X09-433 (Atahualpa), showing geology, gold and alteration indices.

mean values for 10–15 m (and above background for 40 m) beyond the visible alteration zone and beyond the zone of anomalous (>5 ppb) gold. The broad elevation above the background value is not reproduced by the 3K/Al ratio. However, most 3K/Al values are above the coincident background and average values within the zone of anomalous gold, thereby extending the 3K/Al anomaly beyond the visible sericite alteration zone.

Down-hole variations in $(Rb + Cs/Th)_N$ through DH75K09-027 (San Franisco) are compared with background values of 1.6 (average for eight whole-rock analyses of least-altered granodiorite) and mean values of 2.8 (average of all values in the drill hole) in Figure 11. The 3K/Al values are compared with a background value of 0.5 and a mean value of 0.45. As for the Atahualpa drill hole, both indices in DH75K09-027 are well above their respective background and mean values in the three >100 ppb Au zones. The $(Rb + Cs/Th)_N$ and 3K/Al ratios both remain well above background throughout the sericitic alteration zones but only two erratic high $(Rb + Cs/Th)_N$ values were reported beyond the anomalous gold zone (at 185 and 170 m; Figure 11). Similar to the Atahualpa hole, there is no elevation of 3K/Al compared with background, beyond the visible white mica alteration zones.

The new work described here has shown that the alteration indices $(Rb + Cs/Th)_N$ and 3K/Al are maintained above background values in auriferous ore zones (>100 ppb Au). To be really useful as an exploration vector towards mineralisation, an index needs to remain elevated for tens of metres beyond the visible alteration zone and beyond the envelope of anomalous gold (here defined as >5 ppb Au). Only the $(Rb + Cs/Th)_N$ index achieves this result, and only clearly in one of the two holes investigated. In drill hole DH55×09-433 (Atahualpa), the $(Rb + Cs/Th)_N$ index remains elevated 5 to 15 m beyond the anomalous gold zone and the visible sericitic alteration zone (Figure 10). It is interesting to speculate whether a significant gold-bearing vein is present above 110 m in DH55X09-433, where $(Rb + Cs/Th)_N$ values increase to almost 4. Potentially, alteration indices can also be used to vector towards high-grade ore within broad zones of visible alteration and anomalous

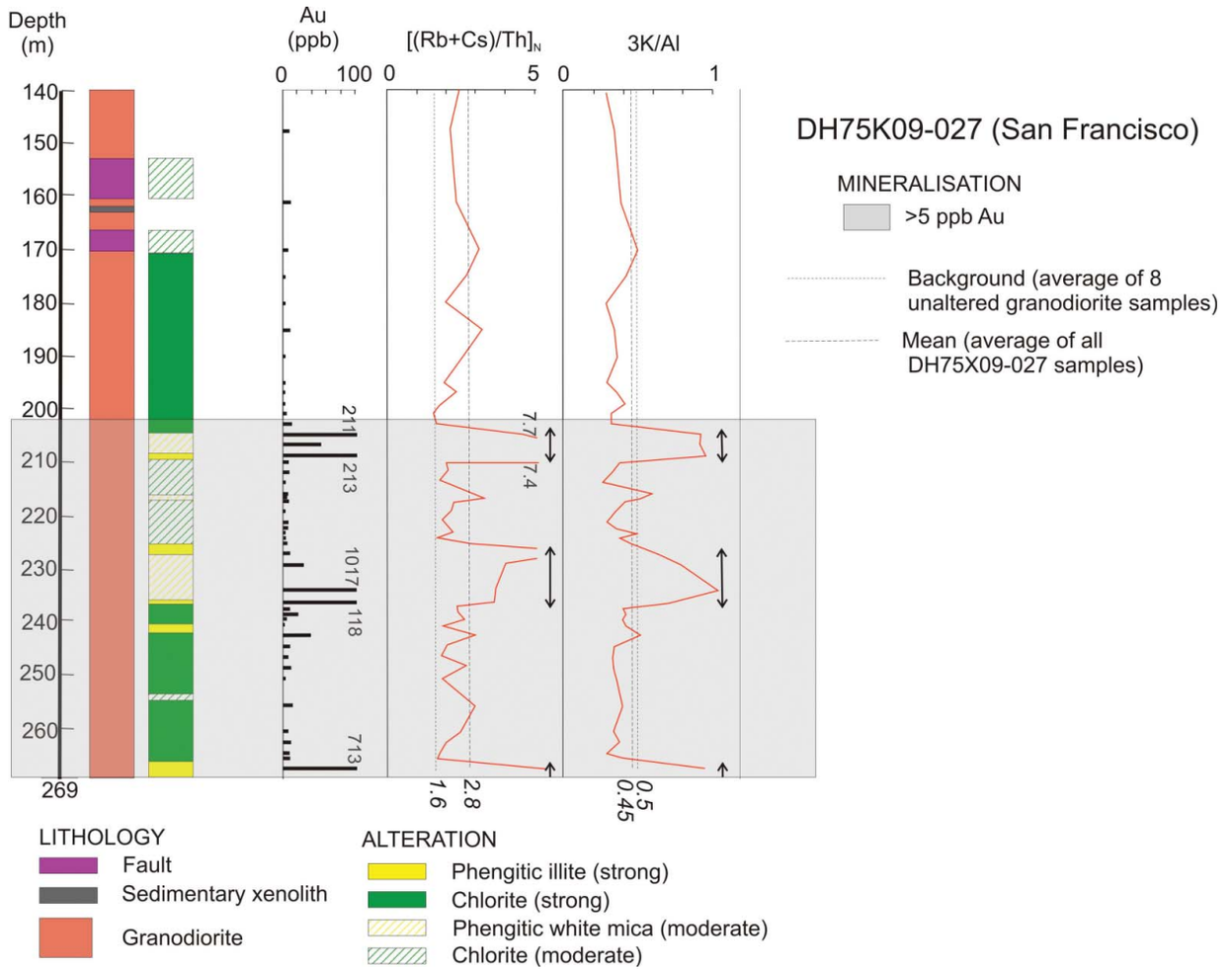

Figure 11 Strip log, drill hole DH75K09-027 (San Francisco), showing geology, gold and alteration indices.

gold. This situation is realised in drill hole DH75K09-027 (San Francisco) where both $(Rb + Cs/Th)_N$ and 3K/Al indices remain higher than the mean value for 8 m above the ore zone at ~235 m.

SUMMARY AND CONCLUSIONS

Exploration targeting techniques for gold in the Pataz district of northern Peru can be applied sequentially from regional to lode scale. At the regional scale, ASTER imagery identifies areas of hydrothermal alteration dominated by hydrated phyllosilicate minerals. One such area extends for tens of kilometres NNW of Vijus and is immediately evident in the ASTER image as an area of abundant AlOH minerals that can be subdivided into domains in which the ~2200 nm absorption feature is characterised by relatively short wavelengths and those that are characterised by relatively long wavelengths (Figure 2). Within this area, outcrops of the Maranon Complex are highly friable and dominated by clay minerals. Around Vijus, at the southern end of this area of argillic alteration, artisanal mining for gold targets quartz–carbonate–sulfide (±barite) veins in faults characterised by intense argillic alteration. SEM analysis of clays from these argillic alteration zones indicates that the clays are predominantly illitic in composition, but locally include kaolinite, possibly produced by weathering of illite. Stable (oxygen, hydrogen) isotope analyses of clays from the argillic alteration zone suggest a magmatic component in the origin of the fluids that caused the hydrothermal alteration. Most of this argillic alteration domain, particularly north of Chicun, is poorly explored and represents an attractive target for gold mineralisation that can be mapped using suitably processed ASTER imagery. Models for shallow level hydrothermal systems (e.g. Hedenquist *et al.* 2000) suggest that the district-scale argillic alteration zone extending NNW from Vijus may be prospective for epithermal gold and carbonate–base metal mineralisation. The occurrence of several artisanal gold workings in the Vijus area, at the southern end of the district-scale zone of argillic alteration provides further support for the validity of this exploration target.

Previous studies of the Pataz–Parcoy gold field show that gold-bearing veins formed during Mississipian (early Carboniferous) ENE–WSW shortening (Haeberlin *et al.* 2004; Witt *et al.* 2009). At the district scale, paleostress mapping (Holyland & Ojala 1997) using a new 1:25 000 geological map of the Pataz district and an ENE–

WSW shortening direction predicts the distribution of domains of low minimum stress (Figure 5). These domains of low minimum stress occupy just 11% of the model area but contain 50% of the known quartz veins, including the mineralised veins hosted by the Pataz batholith. Stress mapping also identifies areas of low minimum stress where veins are not known but are predicted. These represent targets to be followed up with surface rock chip and soil sampling, and exploration drilling.

At the deposit scale, phyllosilicate mineralogy determined by ASD reflectance spectroscopy and SEM mineral analyses shows that the visible proximal but gold-poor sericite alteration envelopes around mineralised batholith-hosted veins are dominated by phengitic hydromuscovite and illite. Mine-scale drilling that intersects intervals of sericite alteration with the characteristic long-wavelength location of the AlOH absorption feature in ASD spectra, but no quartz–carbonate–sulfide veins, may have narrowly missed a mineralised vein with implications for exploration and resource development. Furthermore, ASD hyperspectral analysis of white micas in cryptic alteration beyond the proximal phengitic illite alteration zones can be used to detect shorter wavelength illite or muscovite. Because these minerals are sequentially distributed around the mineralised veins, they can be used as a vector towards gold mineralisation. The ASD spectra can also be used to distinguish between relict phengitic illite, non-phengitic illite and muscovite in zones of chloritic alteration related to the overprinting Cenozoic Andean orogeny.

At the lode scale, sequential analysis of samples from proximal through to distal locations with respect to the mineralised veins shows that pathfinder elements have limited application as a targeting tool because anomalies extend only a few metres beyond visible white mica alteration. By contrast, the $(Rb + Cs/Th)_N$ ratio of Heath & Campbell (2004) is elevated above background values for up to 15 m beyond zones of visible white mica alteration and anomalous gold (>5 ppb), where both are of restricted extent (e.g. less than 15 m in drill hole DH55×09-433, Atahualpa). Although these results cannot be reproduced where visible alteration and anomalous gold define a much broader zone (e.g. >70 m in drill hole DH75K09-027, San Francisco), the $(Rb + Cs/Th)_N$ and 3K/Al (Kishida & Kerrich 1987) can be used as an internal vector toward gold-bearing veins, over a distance of several metres.

ACKNOWLEDGEMENTS

The authors acknowledge the support and encouragement of Compania Minera Poderosa S.A. (CMPSA) in the funding the research presented here and providing excellent assistance in the field. CMPSA also provided processed ASTER imagery and funded geochemical analyses of drill core samples. ASD hyperspectral analysis of drill-core samples was provided by Scott Halley of Mineral Mapping Limited. Julia Kornikova is thanked for her comments on an earlier version of this paper. The paper also benefited from the thoughtful and constructive comments of two anonymous journal reviewers.

REFERENCES

Angeles C. Z. 1994. *Geologia del prospecto Misquichilca*. Unpublished report to Compania Minera Poderosa S. A., 24 pp. plus appendices.

Benavides-Caceres V. 1999. Orogenic evolution of the Peruvian Andes: The Andean cycle. *Economic Geology Special Publication* **7**, 61–107.

Berman M., Bischof L. & Huntington J. 1999. Algorithms and software for the automated identification of minerals using field spectra or hyperspectral imagery. Extended abstract, Thirteenth International Conference on Applied Geologic Remote Sensing, Vancouver, British Columbia, Canada, 1–3 March 1999.

Carillo-Rosúa J., Morales-Ruano S., Esteban-Arispe I. & Hach-Alí P. F. 2009. Significance of phyllosilicate mineralogy and mineral chemistry in an epithermal environment. Insights from the Palai-Islica Au–Cu deposit (Almería, SE Spain). *Clays and Clay Minerals* **57**, 1–24.

Cawood P. A. 2005. Terra Australis Orogen: Rodinia breakup and development of the Pacific and Iapetus margins of Gondwana during the Neoproterozoic and Paleozoic. *Earth Science Reviews* **69**, 249–279.

Corbett G. J. & Leach T. M. 1998. Southwest Pacific rim gold–copper systems: structure, alteration, and mineralization. *Society of Economic Geologists Special Publication* **6**, 237 pp.

Crosta A. P., Ducart D. F., de Souza Filho R., Azevdo F. & Brodie C. G. 2009. Mineral exploration for epithermal gold in NorthernPatagonia, Argentina: From regional- to deposit-scale prospecting using Landsat TM and Terra ASTER. *Reviews in Economic Geology* **16**, 97–108.

Garrels R. M. 1984. Montmorillonite/illte stability diagrams. *Clays and Clay Minerals* **32**, 161–166.

Haeberlin Y., Moritz R. & Fontbote L. 2002. Paleozoic orogenic gold deposits in the eastern Central Andes and its foreland, South America. *Ore Geology Reviews* **22**, 41–59.

Haeberlin Y., Moritz R., Fontbote L. & Cosca M. 2004. Carboniferous orogenic gold deposits at Pataz, Eastern Andean Cordillera, Peru: geological and structural framework, paragenesis, alteration, and $^{40}Ar/^{39}Ar$ geochronology. *Economic Geology* **99**, 73–112.

Heath C. J. & Campbell I. H. 2004. A new geochemical technique for gold exploration: Alkali element mobility associated with gold mineralization in the West Australian Goldfields. *Economic Geology* **998**, 313–324.

Hedenquist J. W., Arribas A. & Gonzalez-Urien E. 2000. Exploration for epithermal gold deposits. *Reviews in Economic Geology* **13**, 245–277.

Holyland P. W. & Ojala V. J. 1997. Computer aided structural targeting: two and three dimensional stress mapping. *Australian Journal of Earth Sciences* **44**, 421–432.

Kasemann S., Meixner A., Rocholl A., Vennemann T., Schmitt A. & Wiedenbeck M. 2001. Boron and oxygen isotope composition of certified reference materials NIST SRM 610/612, and reference materials JB-2G and JR-2G. *Geostandards Newsletter* **25**, 405–416.

Kerrich R. 1987. The stable isotope geochemistry of Au–Ag vein deposits in metamorphic rocks *In*: Kyser T. K. ed. *Short course in stable isotope geochemistry of low temperature fluids*, pp. 287–336. Mineralogical Association of Canada Short Course Series **13**.

Kishida A. & Kerrich R. 1987. Hydrothermal alteration zoning and gold concentration at the Kerr–Adison Archean lode gold deposit, Kirkland Lake, Ontario. *Economic Geology* **82**, 649–690.

Macfarlane A. W., Tosdal R. M., Vidal C. & Paredes J. 1999. Geologic and isotopic constraints on the age and origin of auriferous quartz veins in the Parcoy mining district, Pataz, Peru. *Economic Geology* Special Publication **7**, 267–279.

McCuaig T. C. & Kerrich R. 1998. P–T–t deformation-fluid characteristics of lode gold deposits? Evidence from alteration systematics. *Ore Geology Reviews* **12**, 381–453.

Megard F. 1984. The Andean orogenic period and its major structures in central and northern Peru. *Journal of the Geological Society of London* **141**, 893–900.

Miskovic A., Spikings R. A., Chew D. M., Kosler J., Ulianov A. & Schaltegger U. 2009. Tectonomagmatic evolution of Western Amazonia: Geochemical characterization and zircon U–Pb geochronologic constraints from the Peruvian Eastern Cordilleran granitoids. *Bulletin of the Geological Society of America* **121**, 1298–1324.

Petford N. & Atherton M. P. 1992. Granitoid emplacement and deformation along a major crustal lineament: The Cordillera Blanca, Peru. *Tectonophysics* **205**, 171–185.

Richards J. P., Bray C. J., Channer D. M. & Spooner E. T. C. 1997. Fluid chemistry and processes at the Porgera gold deposit, Papua New Guinea. *Mineralium Deposita* **32**, 119–132.

Rieder M., Cavazzini G., D'yakanov Y. S., Frank-Kamenetskii V. A., Gottardi G., Guugenheim S., Koval P. V., Muller G., Neiva A. M. R., Robert R. L., Sassi F. P., Takeda H., Weiss Z. & Wones D. R. 1999. Nomenclature of the micas. *Mineralogical Magazine* **63**, 267–279.

Rowan L. C. & Mars J. C. 2003. Lithologic mapping in the Mountain Pass, California area using Advanced Spaceborne Thermal Emission and Reflection Radiometer (ASTER) data. *Remote Sensing of Environment* **84**, 350–366.

Rumble D. III. & Hoering T. C. 1994. Analysis of oxygen and sulfur isotope ratios in oxide and sulfide minerals by spot heating with a carbon dioxide laser in a fluorine atmosphrere. *Accounts of Chemical Research* **27**, 237–241.

Schaltegger U., Chew D. & Miskovic A. 2006. Neoproteroszoic to early Mesozoic evolution of the western Gondwana margin: evidence from the Eastern Cordillera of Peru. XIII Congresso Peruano de Geologia, Lima, Octobre, 2006 (extended abstract).

Schreiber D. W., Fontbote L. & Lochmann D. 1990a. Geologic setting, paragenesis, and physicochemistry of gold quartz veins hosted by plutonic rocks in the Pataz region. *Economic Geology* **85**, 1328–1347.

Schreiber D. W., Amstutuz G. C.& Fontbote L. 1990b. The formation of auriferous quartz–sulfide veins in the Pataz region, northern Peru: A synthesis of geological, mineralogical, and geochemical data. *Mineralium Deposita* **25**, 136–140.

Sharp Z. D. 1990. A laser-based microanalytical method for the in-situ determination of oxygen isotope ratios of silicates and oxides: *Geochimica et Cosmochimica Acta* **54**, 1353–1357.

Sharp Z. D., Atudorei V. & Durakiewicz T. 2001. A rapid method for determining the hydrogen and oxygen isotope ratios from water and solid hydrous substances. *Chemical Geology* **178**, 197–210.

Sonntag I., Laukamp C. & Hagemann S. G. 2012. Low potassium hydrothermal alteration in low sulfidation epithermal systems as detected by IRS and XRD. An example from the Co–O mine, Eastern Mindanao, Philippines. *Ore Geology Reviews* **45**, 47–60.

Taylor B. E. 1987. Stable isotope geochemistry of ore-forming fluids. *In*: Kyser T. K. ed. *Short course in stable isotope geochemistry of low temperature fluids*, pp. 337–444. Mineralogical Association of Canada Short Course Series **13**.

Taylor H. P. Jr 1977. Water/rock interaction and the origin of H_2O in granitic batholiths. *Journal of the Geological Society of London* **133**, 509–558.

Vedder W. & McDonald R. S. 1963. Vibrations of the OH ions in muscovite. *Journal of Chemical Physics* **38**, 1583–1590

Vidal C. E., Parades J., Macfarlane A. W. & Tosdal R. M. 1995. Geology and metallogenesis of the auriferous Parcoy mining district, northern Peru. *Boletin de la Sociedad Geologica del Peru*, *Jubilar Alberto Benavides*, 351–377.

Wagner T., Mlynarczk S. J., Williams-Jones A. E. & Boyce A. J. 2009. Stable isotope constraints on ore formation at the San Rafael tin–copper deposit, southeast Peru. *Economic Geology* **104**, 223–248.

Wilson J. J. & Reyes L. 1997. Mapa Geologico Cuadrangulo del Pataz: INGEMMET 1:100 000 Geology Series Map, Quadrangle 16b.

Witt W. K. 1993. Gold mineralization in the Menzies-Kambalda region, Eastern Goldfields, Western Australia. Western Australia Geological Survey, Report 39, 65 pp.

Witt W. K., Hagemann S. G., Villanes C. & Ojala J. 2009. Late Carboniferous orogenic gold and Late Cretaceous to Cenozoic porphyry-related gold associated with the Pataz batholith, northern Peru. SGA Conference, Townsville, Australia, 2009. Extended Abstracts Volume.

Witt W. K., Hagemann S. G., Villanes C., Sologuren D., Vennemann T., Zwingmann H. & Jourdan F. 2011. A > 3 km vertical section through mesothermal to epithermal levels of a Carboniferous, alkali intrusion-related hydrothermal system in the Eastern Andean Cordillera, Pataz, northern Peru. SGA Conference, Antafogasta, Chile, 2011, Extended Abstracts Volume.

Witt W. K., Hagemann S. G., Villanes C. & Qingtao Zeng 2013. New geochronological results and structural evolution of the Pataz gold mining district: implications for the timing and origin of the batholith-hosted veins. *Ore Geology Reviews* **50**, 143–170.

SUPPLEMENTARY PAPERS

Table 1 Results of XRD analysis of samples from Vijus-Santa Filomena area.

Table 2 SEM analyses of white mica and clay minerals from mineralised quartz–carbonate–sulfide veins, Viju-Santa Filomena area.

Table 3 Results of stress modelling, Pataz district.

Table 4 SEM analyses of white mica and clay, batholith-hosted proximal alteration.

Table 5 Average and range of selected elements from 8 whole-rock geochemical samples of granodiorite from the Pataz district.

Received 13 April 2012; accepted 4 November 2012